Potent Apoptotic Response Induced by Chloroacetamidine Anthrathiophenediones in Bladder Cancer Cells

Susanna Cogoi,[†] Sonia Zorzet,[‡] Andrey E. Shchekotikhin,[§] and Luigi E. Xodo*[,†]

[†]Department of Medical and Biological Sciences, University of Udine, P.le Kolbe 4, 33100 Udine, Italy

[‡]Department of Life Science, University of Trieste, Via Giorgieri 7-9, 34100 Trieste, Italy

[§]Gause Institute of New Antibiotics, B. Pirogovskaya, 11, Moscow 119021, Russia

Ⓢ *Supporting Information*

ABSTRACT: We previously found that two neighboring G-quadruplexes behave as a molecular switch controlling the expression of *HRAS* (Cogoi, S.; Schekotikhin, A. E.; Xodo, L. E. *Nucl. Acids Res.* **2014**, DOI: 10.1093/nar/gku574). In this study we have designed anthrathiophenediones with two chloroacetamidine-containing side chains (CATDs) as G-quadruplex binders and have examined their anticancer activity in T24 bladder cancer cells bearing mutant *HRAS* and in T24 xenografts. The designed CATDs (**3a−e**), bearing alkyl side chains of different length, penetrate T24 cancer cells more than their analogues with guanidine-containing side chains. The lead compounds **3a** and **3c** inhibit *HRAS* expression, metabolic activity, and colony formation in T24 cancer cells. They also activate a strong apoptotic response, as indicated by PARP-1, caspases 3/7, and annexin V/propidium iodide assays. Apoptosis occurs under conditions where cyclin D1 is down-regulated and the cell cycle arrested in G2 phase. Finally, compound **3a** inhibits the growth of T24 xenografts and increases the median survival time of nude mice.
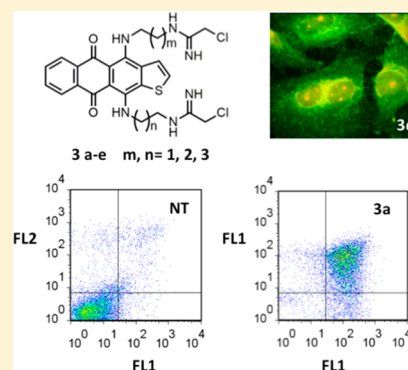
Anthraquinone based drugs such as adryamicyn and mitoxantrone are clinically used in anticancer therapies.[1] Early studies suggested that these compounds have anticancer activity because of their capacity to bind to DNA.[2,3] The past years have witnessed an intensive search for new anthraquinone derivatives with enhanced biological activity.[4a−c] In 1997, Hurley and Neidle discovered that human telomerase was inhibited by diamidoanthraquinones and they proposed a suggestive mechanism of action based on the binding of the molecule to non-B DNA G-quadruplex structures assumed by the guanine repeats of the telomeres.[5,6] Later studies strengthened the G-quadruplex hypothesis, pointing out that several other molecules including acridines, fluorenones, and tetracyclic benzonaphthofurandione showed telomerase activity.[7a−c] Neidle and co-workers reported that important determinants for enhancing the binding of anthraquinones to quadruplex DNA are the introduction of side chains, each with a terminal cationic group, as well as the extension of the tricyclic chromophore.[8] In a previous work we have expanded the anthraquinone chromophore by fusing its aromatic tricyclic surface to a thiophene ring in order to obtain a tetracyclic core that should extend $\pi-\pi$ stacking interactions with a planar G-tetrad of quadruplex DNA.[9] We also introduced two alkyl side chains terminating with a cationic guanidine group with the aim to promote interactions with the phosphates in the loops or grooves of the G-quadruplex. We discovered that the guanidine-containing anthrathiophenediones enhanced the affinity for G4-DNA as they increased the T_M of quadruplex Htelo up to 30 K,[9] while, for instance, aminoacyl anthraquinones increased the T_M up to 9.8 K.[10] We also found that the alkylguanidine side chains influenced not only the quadruplex stability but also the cellular uptake.[9,11] We have reported that the cellular uptake of guanidine-containing anthrathiophenediones depends on the length of the alkyl spacer in the side chains. The most hydrophobic analogues (with three or four methylene groups) were transported into the cells mainly by passive diffusion, while the compound with shorter side chains (with two methylene groups), entered T24 cancer cells by an active transport (endocytosis).[9] However, as the guanidine group is a very strong base in water ($pK_a = 13.6$), it assumes a positive charge that is highly stabilized by resonance under physiological conditions. This stable charge may reduce the uptake. So we reasoned that the substitution in the alkyl side chains of the terminal guanidine groups with chloroacetamidines, which are more lipophilic and hold positive charges less stabilized by resonance, should improve the uptake. We therefore designed a series of 4,11-bis[ω-(chloroacetamidine)alkylamino]anthra[2,3-*b*]thiophene-5,10-diones (CATDs) (**3a−e**) (Scheme 1) and examined their activity in T24 bladder cancer cells bearing a mutant *HRAS* allele. We found that the designed CATDs penetrate cancer cells much more efficiently than their guanidine-containing analogues. They also display a high affinity for the G-quadruplexes formed by the regulatory GC-elements of the *HRAS* promoter, located upstream of the main transcription start sites. We report that these molecules

Scheme 1. Synthesis of CATDs 3a−e[a]
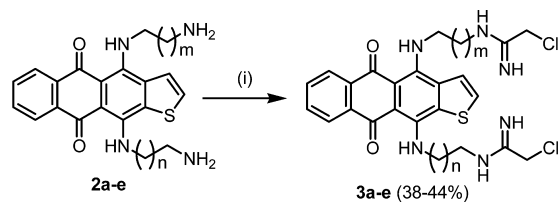
2a, 3a m=n=1; **2b, 3b** m=1, n=2; **2c, 3c** m=2, n=1; **2d, 3d** m=n=2; **2e, 3e** m=n=3.

[a]Reagents and conditions: (i) ethyl 2-chloroacetimidate hydrochloride, EDIA, DMSO, 40 °C, 5 h.

caused a total extinction of *HRAS* and the inhibition of colony formation in bladder cancer cells. Contrary to the guanidine-containing analogues, the lead compounds **3a** and **3c** promoted a strong apoptotic response as a consequence of the blockade of the cells in the G2 phase. Finally, the lead compound **3a**, which showed the highest activity in vitro, unveiled a good capacity to slow the growth of a T24 tumor xenograft and significantly increase the median survival time of nude mice. Together, our results indicate that the designed CATDs have a potential as anticancer drugs for bladder tumors harboring mutant *HRAS* alleles.

■ RESULTS AND DISCUSSION

Synthesis of CATDs (3a−e). For the preparation of new derivatives of 4,11-diaminoanthra[2,3-*b*]thiophene-5,10-diones a previously developed methodology was applied.[9,11,12] The starting homologues **2a−e** with side chains of different length have been obtained by a nucleophilic substitution of the alkoxy groups of 4,11-dibutoxyanthra[2,3-*b*]thiophene-5,10-dione with the corresponding diaminoalkanes.[9,12] The terminal amino groups of **2a−e** were transformed into chloroacetamidines by treatment with ethyl 2-chloroacetimidate hydrochloride, yielding the corresponding 4,11-bis[ω-(chloroacetamidine)-alkylamino] derivatives **3a−e** (Scheme 1).

The new compounds **3a−e** have been purified by reverse-phase chromatography, followed by reprecipitation. The purified CATDs gave analytical and spectroscopic data in full accordance with their assigned structures (Materials and Methods). The purified compounds have been used for in vitro and in vivo studies.

Activity of Designed CATDs in Bladder Cancer Cells. Urinary T24 bladder cancer cells harbor a mutant *HRAS* allele. The proliferation of these cells strongly depends on the expression of the oncogenic *HRAS* allele, which encodes for an altered protein (p21^RAS) that transmits constitutively downstream signals for cell proliferation, a behavior favoring the malignant transformation of the cells. Bladder cancer cells are addicted to oncogenic *HRAS* in the same way as pancreatic cancer cells are addicted to mutant *KRAS*. It has been reported that the *RAS* oncogenes remodulate the metabolic pathways of cancer cells to fuel their higher proliferation rate.[13,14] For this reason the *RAS* genes are attractive targets for anticancer drugs. Recently, we have discovered that the expression of *HRAS* is controlled by two neighboring G-quadruplexes, located upstream of the major transcription start sites and behaving as a molecular switch.[15,16] We hypothesized that small molecules binding to the G-quadruplexes and locking the promoter into the nontranscriptionally active form should make extinct oncogenic *HRAS* in cancer cells and inhibit cell growth. To this end we have designed a new class of anthrathiophene-

diones (**3a−e**) as G-quadruplex binders. We first tested if these molecules showed a different activity in T24 cancer cells, which are addicted to oncogenic *HRAS*, and 293 noncancer cells, which instead harbor only wild-type *HRAS* alleles. The metabolic activity in T24 and 293 cells exposed for 72 h to increasing amounts of compounds **3a−e** is reported in Figure 1A. For each compound we determined the IC$_{50}$ (Table 1). As
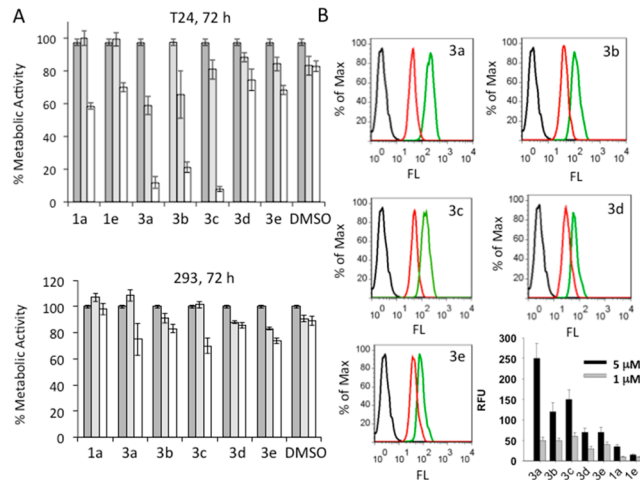

Figure 1. (A) The % metabolic activity of T24 cancer and 293 noncancer cells treated with 0 (dark gray), 1 (gray), and 5 (white) μM CATDs **3a−e** and guanidine analogues **1a** and **1e**, for 72 h. (B) FACS analysis of T24 cancer cells treated with 1 (red line) and 5 (green line) μM CATDs **3a−e** and guanidine analogues **1a** and **1e**, for 4 h. The histogram shows the fluorescence of the cells (RFU, relative fluorescence unit) due to the internalization of CATDs and guanidine analogues **1a** and **1e**.

can be seen, while the designed compounds reduced the metabolic activity of *HRAS* mutant T24 cancer cells, they showed a significantly lower effect on 293 noncancer cells. The data also show that the less lipophilic compounds **3a**, **3b**, and **3c**, bearing shorter alkyl side chains, are more efficient effector molecules than the more lipophilic **3d** and **3e**, bearing longer side chains (Scheme 1). The different cytotoxic effect caused by the designed CATDs in cancer and noncancer cells is in keeping with our working hypothesis and induced us to evaluate the anticancer activity of the new compounds both in vitro and in vivo focusing on their mechanism of action.

Uptake of the Designed CATDs in Cancer and Noncancer Cells. A basic property of an anticancer drug designed to bind to a genomic target is its capacity to penetrate the cell membranes and access the nucleus with a high efficiency. As CATDs emit red fluorescence when they are excited at 560 nm (Supporting Information, Figure S1), their cellular uptake was investigated by FACS. Figure 1B shows a typical FACS analysis of T24 cells incubated for 4 h with the compounds **3a−e** at the concentration of 1 or 5 μM (preliminary experiments as a function of time showed that the uptake is maximum after 4 h of incubation). The data show that in the presence of CATDs the fluorescence associated with the cells strongly increases (the peak shifts to the right) as a result of the drug internalization. The fluorescence of the cells treated with 1 or 5 μM **3a−e** and with the guanidine-containing analogues **1a** and **1e** (Supporting Information, Figure S2) have been measured and the data displayed in a histogram. The uptake is inversely proportional to the length of the alkyl side

Table 1. IC$_{50}$ (μM)^a of the Designed CATD Compounds in T24 Cancer and 293 Noncancer Cells

cell	3a	3b	3c	3d	3e	1a	1e
T24	2.7 ± 0.2	2.9 ± 0.01	3.0 ± 0.02	6.8 ± 0.5	11.5 ± 0.4	4.4 ± 0.2	19.1 ± 3.6
293	6.4 ± 0.7	10.1 ± 0.2	12.6 ± 0.4	19.4 ± 3.4	>30	>30	>30

^{a}The values have been determined by a resazurin assay after the compounds (from 1 to 30 μM) have been incubated with the cells for 72 h.

chains, i.e., to the lipophilicity of the molecules, as previously observed for the guanidine-containing analogues.[9] This suggests that these molecules should be transported into the cells by a mechanism more complex than the passive diffusion. As we expected, the designed CATDs showed a significantly higher uptake than the guanidine-containing analogues **1a** and **1e**. For instance, **3a** ($n = 1$, $m = 1$) and **3e** ($n = 3$ and $m = 3$) at 5 μM are taken up ~5-fold more than the corresponding **1a** ($n = 1$, $m = 1$) and **1e** ($n = 3$ and $m = 3$), suggesting that the substitution in the side chains of the guanidine groups with chloroacetamidines strongly increases the cellular uptake. We also compared in T24 cells the uptake of **3a** and **1a**, which have side chains of the same length but different terminal groups, and found that the former is taken up more efficiently than the latter, at various concentrations (Figure 2A). Additionally, we
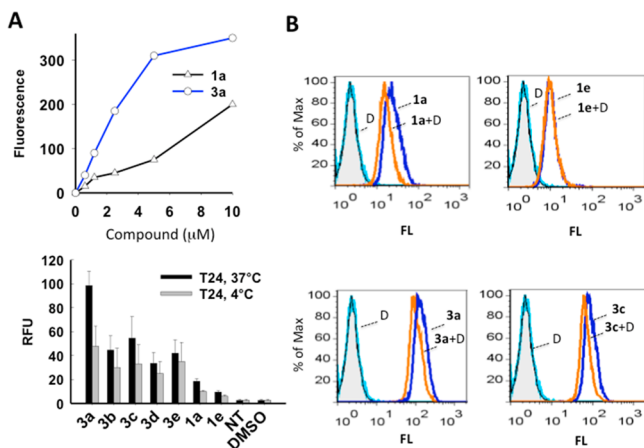

Figure 2. (A) (Top panel) Uptake by T24 cancer cells of compounds **1a** and **3a** incubated for 4 h; (bottom panel) uptake by T24 cancer cells of 5 μM CATDs **3a−e**, **1a**, and **1e** incubated for 4 h at 4 and 37 °C. (B) FACS analysis of T24 cancer cells treated with 5 μM **1a**, **1e**, **3a**, and **3c** for 4 h in the presence and absence of 80 μM dynasore (D).

found that the uptake is lower at 4 °C than 37 °C, in particular with the less lipophilic **3a**, **3b**, and **3c** (Figure 2A) and that T24 bladder cancer cells take up the designed CATDs about 2-fold more efficiently than 293 noncancer cells (Supporting Information, Figure S3). The temperature dependence of the uptake of less lipophilic **3a**, **3b**, and **3c** suggests that these molecules may penetrate the cell membrane by passive diffusion and active transport. The presence of an active transport is supported by the fact that when T24 cancer cells are incubated at 37 °C in the presence of dynasore (an inhibitor of dynamin, a protein that inhibits the budding of endocytotic vesicles from the membranes[17−19]), the uptake of **3a** and **3c** is slightly inhibited, suggesting that the two chloroacetamidine compounds should be transported into the cells also by endocytosis (Figure 2B). A similar behavior has been previously observed with **1a** but not with more lipophilic **1e**.[9]

As FACS analyses cannot discriminate between surface bound fluorescence or translocated fluorescence, we used confocal microscopy to find out if the designed CATDs internalize into the cells. Figure 3 (left panel, top row) shows
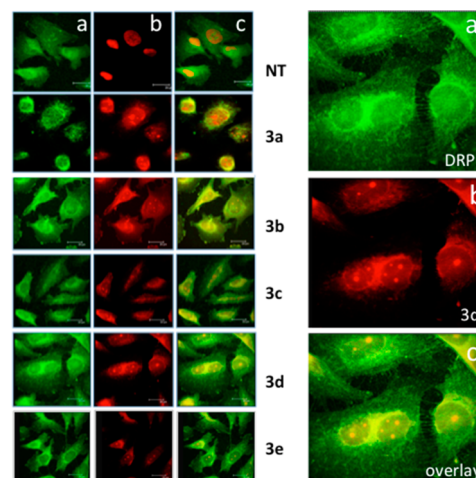

Figure 3. (Left) Confocal microscopy images of T24 cells treated with 5 μM CATDs **3a−e** for 4 h. (Right) Magnification of images relative to cells treated with compound **3d**. For untreated cells, the cytoplasm was stained with antibody DRP1 and the nucleus with propidium iodide. For treated cells, the cytoplasm was stained in green with antibody DRP1 and red fluorescence shows the CATD localization.

T24 untreated cancer cells with the cytoplasm stained by immunofluorescence with anti dynamin-related protein 1 (DRP-1) antibody (green fluorescence, panel a). The nucleus of the cells was stained with propidium iodide (red fluorescence, top panel b). The overlay, panel c, shows both cytoplasm and nucleus of the cells. As compounds **3a−e** emit red fluorescence, their presence in the cells is detected by irradiation with a laser at 543 nm (panel b, from second row to bottom). The panels (a, b, c) show confocal images (Z-axis sections at 0.1 μm intervals) of T24 cells treated for 4 h with the designed compounds. The images show that the designed CATDs localize both in the cytoplasm and nucleus. The images obtained with compound **3d** appeared particularly clear and informative (Figure 3, right). The green fluorescence of DRP1-1 is localized in the cytoplasm, in particular in the perinuclear region.[20,21] The red fluorescence of compound **3d** is located in the nucleus and perinuclear region. The granular distribution in the nucleoplasm suggests that a fraction of compound **3d** accumulates in the nucleoli as well. As for the other compounds, their behavior is roughly similar to that of **3d**. Taken together, the FACS and confocal microscopy data show that the designed chloroacetamidine compounds are taken up by T24 bladder cancer cells more efficiently than the corresponding guanidine-containing analogues and that they internalize both in the cytoplasm and nucleus/nucleoli.

The Designed CATDs Bind to the *HRAS* G-Quadruplexes and Show G4-to-Duplex Specificity. We have previously demonstrated that two neighboring G-rich sequences, located at the transcription start site, regulate *HRAS*

3

transcription: when they are folded into the G-quadruplex form, the promoter is not transcriptionally active. In contrast, when the G-quadruplexes are bound and unfolded by MAZ, a zinc-finger transcription factor, the promoter assumes a canonical B-DNA conformation and activates transcription (Figure 4A).[15] Therefore, small molecules that stabilize the G-
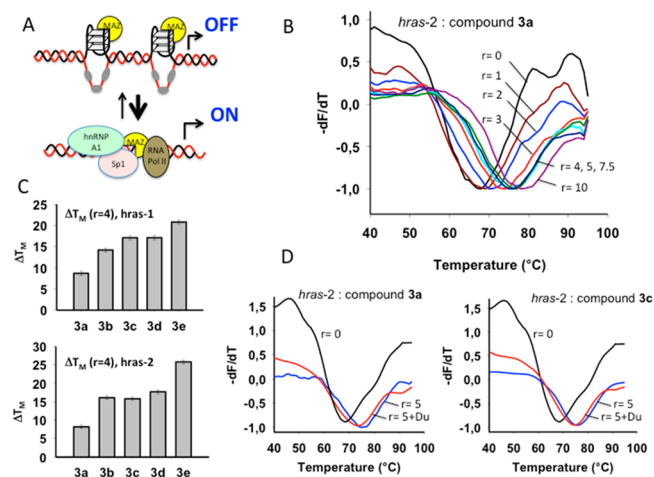

Figure 4. (A) Putative molecular switch proposed for the regulation of the *HRAS* gene. The *HRAS* promoter at the G-rich elements is folded into G-quadruplex structures that maintain transcription to a basal level. Transcription is activated when MAZ unfolds the G-quadruplexes and the promoter assumes the canonical B-DNA conformation. (B) Typical FRET-melting for G-quadruplex *hras*-2 (excitation 470 ± 20 nm, emission 522 ± 7 nm) in the presence of increasing amount of **3a** (from $r = 0$ to $r = 10$, the T_M values are 68.1, 68.7, 70.8, 73.4, 75.6, 75.8, 76.5, 78.5 °C, respectively). Experiment is done in 50 mM Tris-HCl, pH 7.4, 10 mM KCl. (C) T_M increase (ΔT_M) of G-quadruplexes *hras*-1 and *hras*-2 caused by the designed CATDs at $r = 4$ ($r = [\text{CATD}]/[\text{G4}]$). (D) FRET-melting competition assay (excitation 470 ± 20 nm, emission 522 ± 7 nm) to evaluate the G-quadruplex-to-duplex specificity of compounds **3a** and **3c**. Experiment is done in 50 mM Tris-HCl, pH 7.4, 10 mM KCl: G4 (black curve); G4 + **3a** or **3c** ($r = 5$) (blue curve); G4 + **3a** or **3c** ($r = 5$) + 10-fold duplex (Du) (red curve).

quadruplexes and inhibit the action of MAZ are expected to down-regulate transcription.[9,15] To examine the binding of CATDs to the *HRAS* G-quadruplexes, we carried out fluorescence resonance energy transfer (FRET) experiments. The quadruplex-forming sequences *hras*-1 and *hras*-2 have been labeled at the 5′ and 3′ ends with carboxyfluorescein and tetramethylrhodamine. Since the designed compounds absorb in the region where the fluorophores emit light, the binding of **3a**−**e** to the *HRAS* G-quadruplexes has been investigated by fluorescence quenching titrations. A typical titration is reported as additional data (Supporting Information, Figure S4). From the titration experiments we obtained for each CATD the binding curves for the two G-quadruplexes. The curves have been best-fitted to the Hill equation $y = aL^n/(K_d + L^n)$, where L is the fraction of bound ligand, K_d the dissociation constant, and a a constant of proportionality (SigmaPlot 11, Systat Software). The analyses gave K_d values between 10^{-8} and 10^{-9} M (Table 2). The stabilizing effect on the G-quadruplexes promoted by the designed CATDs was determined by FRET-melting experiments. Typical melting curves of quadruplex *hras*-2 in the presence of increasing concentrations of compound **3a** are shown in Figure 4B. The T_M of the

Table 2. Dissociation Constants for the Interactions between CATDs and *hras*-1 and *hras*-2 Quadruplexes[a]

CATD	K_D (nM), *hras*-1	n [b]	K_D (nM), *hras*-2	n [b]
3a	611 ± 469	1	317 ± 31	1.7
3b	179 ± 58	1	221 ± 19	2.3
3c	178 ± 20	1	168 ± 10	1
3d	260 ± 15	1	276 ± 67	1.2
3e	231 ± 12	2.9	215 ± 9	3.4

[a]Data have been obtained in 50 mM Tris-HCl, pH 7.4, 100 mM KCl (*hras*-1), or 10 mM KCl (*hras*-2). [b]n = Hill coefficient.

quadruplex increases with r (where $r = [\text{CATD}]/[\text{G4-DNA}]$) from 67.2 at $r = 0$ to 78.5 °C at $r = 10$. The increase of T_M (ΔT_M) induced by the designed CATDs on quadruplexes *hras*-1 and *hras*-2 (at $r = 4$) is reported in Figure 4C. It is found that ΔT_M increases with the length of the alkyl spacer in the side chains. This can be explained by the fact that longer alkyl chains improve the interactions of the terminal cationic groups with the phosphates in the grooves or loops of the G-quadruplexes. The ΔT_M induced by CATDs on quadruplex *hras*-1 spans from 9 to 20 °C, while on quadruplex *hras*-2 ΔT_M spans from 7 to 25 °C. We also investigated the quadruplex-to-duplex specificity of the designed CATDs by melting the quadruplex *hras*-2 in the presence of **3a** or **3c** and an excess of duplex DNA. We set up a FRET competition experiment with a 10-fold excess duplex over the quadruplex. The result showed that the T_M of the quadruplex *hras*-2 changed only slightly upon addition of the duplex competitor (Figure 4D). The quadruplex in 10 mM KCl had a T_M of 68.1 °C, which increased in the presence of 5 equiv of **3a** or **3c** ($r = 5$) up to 75.6 and 75.8 °C, respectively. After addition of 10-fold excess duplex, the T_M values remained roughly the same (variation of ±1 °C), suggesting that the two molecules exhibit a satisfactory quadruplex-to-duplex specificity which allows their use in G4 targeted cell based experiments. To investigate the activity of the designed CATDs in T24 cancer cells we focused on compounds **3a** and **3c**, as they show the highest capacity to inhibit the metabolic activity in cancer cells. We also used the guanidine-containing analogues **1a** and **1e** for comparison.

Compounds 3a and 3c Inhibit *HRAS* and Colony Formation in Bladder Cancer Cells. A first assessment of the capacity of compounds **3a** and **3c** to inhibit *HRAS* expression was obtained by quantitative real-time PCR. We determined the level of *HRAS* mRNA in T24 bladder cancer cells treated for 6 and 24 h with 5 μM **3a**, **3c**, **1a**, and **1e** (Figure 5A). At both times **3a** and **3c** significantly reduced *HRAS* mRNA compared to housekeeping gene β2-microglobulin to 35% and 45% of the control (untreated cells) after 6 h and to 34% and 24% of the control after 24 h. The guanidine analogues **1a** and **1e**, which enter the cells less efficiently than CATDs, caused a weaker inhibition. We also measured by immunoblotting the amount of protein p21$^{\text{RAS}}$ expressed in the untreated and CATD-treated cells and found that compounds **3a** and **3c** strongly reduced the protein level. As the half-life of the ras proteins is in the range between 24 and 36 h,[22,23] we determined the level of p21$^{\text{RAS}}$ 48 h after treatment with **3a** and **3c** (Figure 5B). It can be seen that **3a** at 2.5 and 5 μM causes a dramatic drop of the level of p21$^{\text{RAS}}$ up to ~4% of the control (untreated cells), whereas **3c** showed inhibitory activity only at 5 μM (~40% of the control). The reference guanidine-containing compounds **1a** and **1e** at the concentration of 5 μM

Figure 5. (A) Quantitative real-time quantification of *HRAS* mRNA 6 and 24 h after treatment with 5 μM **1e**, **1a**, **3a**, and **3c**. The % *HRAS* mRNA was determined by measuring the ratio (*HRAS* mRNA)/(β2-microglobulin mRNA) in treated (T) and untreated (C) T24 cancer cells: % *HRAS* mRNA is given by (T/C) × 100. (B) Western blots of cellular lysates obtained from T24 cells untreated or treated with 2.5 (top) and 5 μM (bottom) **1e**, **1a**, **3a**, and **3c**, 48 h following treatment. The % residual p21^{RAS} was determined by measuring the ratio (p21^{RAS})/(β-actin) in treated (T) and untreated (C) T24 cancer cells. The % residual p21^{RAS} is given by (T/C) × 100.

Figure 6. (A) Dual luciferase assay with plasmid pHRAS-luc, bearing the wild type HRAS promoter, and the mutant plasmid Mut-A (bearing the point mutations *a* and *c*) and Mut-B (bearing the point mutations *b* and *c*) in which the G-quadruplexes cannot be formed. T24 cells have been first treated for 4 h with 100 and 200 nM **3a**, then transfected with the expression vectors. The ordinate of the histogram reports (T/C) × 100, where T = (firefly luciferase)/(*Renilla* luciferase) of the cells treated with compound **3a**, C = (firefly luciferase)/(*Renilla* luciferase) of the untreated cells. (B) Colony forming assay of T24 cancer cells treated with 1 μM **1a**, **1e**, **3a**, and **3c**. Colonies have been fixed and stained with methylene blue, 7 days after cell treatment. The histogram shows the percentage of colony formation of the treated cells compared to untreated cells. Difference from control is sustained by Student's *t* test: (∗) $p < 0.01$.

reduce p21^{RAS} roughly in the same way as **3c** but to a much lower extent than **3a**.

To demonstrate that the compounds inhibit the expression of *HRAS* through their binding to the *HRAS* G-quadruplexes, we performed a luciferase experiment with compound **3a**. We used an expression vector (pHRAS-luc) where firefly luciferase was driven by the *HRAS* promoter and two mutant vectors (Mut-A and Mut-B) where the two neighboring G-quadruplexes *hras*-1 and *hras*-2 were destabilized by four point mutations: Mut-A contains point mutations *a* and *c*, while Mut-B contains point mutations *b* and *c* (Figure 6A).[15] The assay was performed with T24 cells that have been first treated for 4 h with 100 or 200 nM compound **3a**, then transfected with pHRAS-luc or Mut-A or Mut-B and pRL-CMV (a *Renilla* luciferase vector driven by CMV promoter) to determine the transfection efficiency. After 48 h we measured the ratio *f/R* (*f* = firefly luciferase and *R* = *Renilla* luciferase) in the cells untreated and treated with **3a**. Compound **3a** reduced firefly luciferase expressed by pHRAS-luc to ~40% of the control, while it did not reduce luciferase from mutant Mut-A and Mut-B. This suggests that the inhibition of luciferase observed with wild type pHRAS-luc is mediated by the binding of **3a** to the G-quadruplexes.[15]

As protein HRAS activates a downstream pathway stimulating mitosis, its extinction by compounds **3a** and **3c** should affect cell proliferation. To test this, we have carried out a colony formation assay. The number of colonies formed by T24 bladder cancer cells after an incubation of 7 days in a medium with and without CATDs is reported in Figure 6B. It can be seen that compounds **3a** and **3c** completely blocked the formation of the colonies, while the less penetrating **1a** and **1e** analogues did so to a much lower extent.

Compounds 3a and 3c Induce a Potent Apoptotic Response in T24 Bladder Cancer Cells. The strong antiproliferative activity exhibited by **3a** and **3c** raised the question whether the arrest of cell growth promoted by these compounds might be due to apoptosis. It is known that during the execution phase of apoptosis, PARP-1 is specifically cleaved by the caspases producing a C-terminal fragment of 24 kDa and a shorter protein of 89 kDa. This should inactivate PARP-1 and thus prevent survival by the DNA repair machinery.[24] By using a specific antibody recognizing both cleaved and uncleaved PARP-1, we found by immunoblotting that **3a** and **3c** caused a massive cleavage of PARP-1 (~80% of the protein) at 48 h while the guanidine-containing analogues **1a** and **1e** did not (Figure 7A). To confirm that **3a** and **3c** actually cause apoptosis, we measured the activation of caspases 3/7 by Apo-ONE assay (Figure 7B). It is found that compounds **3a** and **3c** but not **1a** increased up to 15-fold the caspase activation, in keeping with the PARP-1 cleavage data. An additional assessment of apoptosis induced by **3a** and **3c** was obtained by annexin V−propidium iodide assays. In early apoptosis, the cell membrane loses its phospholipid asymmetry and phosphatidylserine (PS) normally located in the inner leaflet jumps into the outer leaflet. As annexin V shows a high affinity for PS, annexin V−FITC can mark the cells in early apoptosis. By contrast, late apoptotic or necrotic cells, being permeable to annexin V and PI, are stained by both dyes. Figure 7C shows a FACS analysis performed after treatment of T24 cells with **3a**, **3c**, **1a**, and **1e**. The results are reported in a histogram and as additional data (Supporting Information, Table S5). The percentage of apoptotic cells is 13 ± 5% in untreated or **1a**/**1e**-treated cells, while it is 88 ± 1% and 81 ± 5% in the cells treated with **3a** and **3c**, respectively. Interestingly, the two
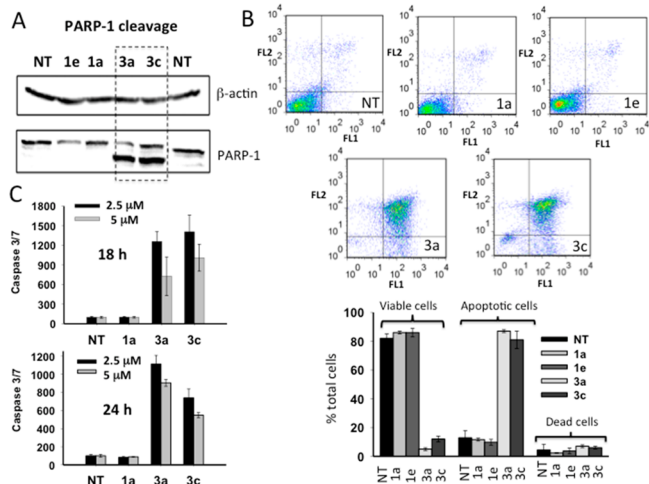
5

Figure 7. (A) PARP-1 is cleaved in T24 cancer cells treated with 2.5 μM **1a**, **1e**, **3a**, and **3c**. (B) Propidium iodide/annexin V assay for the detection of early and late apoptotic T24 cancer cells, 24 h after treatment with 2.5 μM **1a**, **1e**, **3a**, and **3c**. The histogram shows the percentage of viable, apoptotic, and dead cells after treatment. (C) Apo-ONE assay showing caspase 3/7 activation in T24 cancer cells 18 and 24 h after treatment with 2.5 and 5 μM **1a**, **1e**, **3a**, and **3c**.

Figure 8. (A) FACS analysis of untreated and treated (**1a**, **1e**, **3a**, and **3c**) T24 cancer cells showing the fractions of cells in various phases of the cell cycle. The analysis, conducted 48 h after treatment, shows that the cells are blocked in G2. (B) Western blots showing the levels of cyclin D1 48 h following treatment with the 2.5 μM **1a**, **1e**, **3a**, and **3c**. (C, left panel) Effect of compound **3a** intratumorally injected in nude mice bearing a subcutaneous T24 xenograft. The ordinate axis reports the growth of the tumor xenograft (mg). The treatment (1.7 mg/kg of **3a**) was performed four times at days 1, 8, 15, and 22. Each group (treated and untreated) comprises eight mice. From day 8, after the second treatment, the T24 xenograft grew more slowly than in the nontreated mice group ($P < 0.05$). From day 15, after the third treatment, $P < 0.001$. (C, right panel) Kaplan−Meier curves showing the effect of compound **3a** compared to the untreated group. The median survival time of the group treated with **3a** is 54 days, statistically higher than the median survival time of the control group (32 days).

chloroacetamidine molecules activate a strong apoptotic response in T24 bladder cancer cells while the two guanidine-containing analogues did not. Next, we asked how the designed CATDs activate apoptosis. Previous studies have reported that anthraquinone derivatives such as adriamycin, epirubicin, and daunomycin induce apoptosis by the generation of ROS.[25−27] From a chemical point of view, the quinone system, being an electron acceptor, could interact with molecular oxygen and generate superoxide anion.[28] We therefore measured the intracellular ROS level in treated and untreated T24 bladder cancer cells (cellular ROS detection kit, Abcam). When the cells were exposed for 24 h to 1 and 5 μM **3a** or **3c**, we did not observe any increase of ROS compared to the untreated cells (not shown). So the designed CATDs **3a** and **3c** induced apoptosis via a ROS-independent pathway. To find out how apoptosis is activated by CATDs, we analyzed the cell cycle by FACS, as well as the level of cyclin D1, a protein essential for cell cycle progression and proliferation.[29,30]

The Designed CATDs Repress Cyclin D1 and Arrest Cancer Cells in the G2-Phase. The mammalian cell cycle consists of four phases G1, S, G2, and M, and dysregulations of the cell cycle progression are typical of cancer. A central role in cell cycle progression is played by cyclin D1.[29,30] It has been demonstrated that variations in cyclin D1 levels throughout the cell cycle are essential for cell proliferation.[31] The expression of cyclin D1 is dependent on proliferative signals and RAS activity.[32,33] The RAS proteins are growth-factor sensitive molecules that behave as a cellular switch for the activation of several processes including mitosis. They activate a cascade of kinases that induce the expression of cyclin D1 and cell proliferation.[34] To investigate if there is a correlation between *HRAS*, cyclin D1, and the cell cycle, we analyzed by FACS the cell cycle of T24 cells untreated or treated with compounds **3a** and **3c** and with the guanidine-containing analogues **1a** and **1e** for 48 h (Figure 8A,B) and 72 h (Supporting Information, Figure S6). The results show that both **3a** and **3c**, but not **1a** and **1e**, arrest the cells in the G2 phase of the cell cycle. In fact, after 48 h, the cell population in G2 increases from 18.5% in the
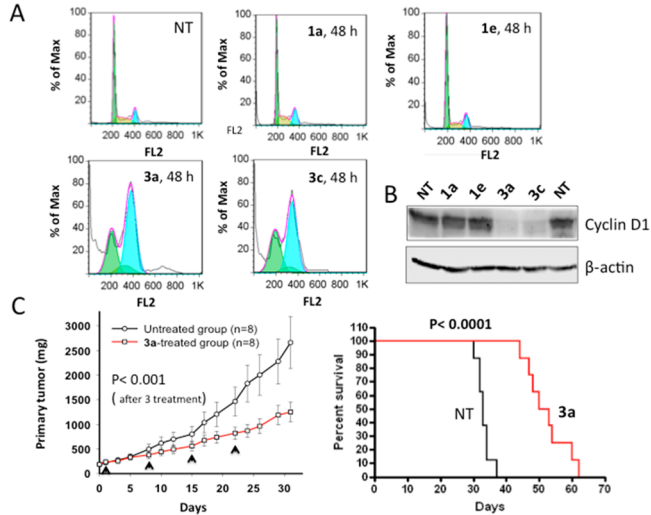
untreated cells to 72.2% and 66.0% in the cells treated with **3a** and **3c**, respectively. The population in G1 decreased from 52.4% to 12.2% and 28.9%. At 72 h following treatment with **3a** and **3c**, the percentage of cells in G2 increased from 17.7% to 44.7% and 83.0%, respectively (Supporting Information, Figure S6). Compounds **1a** and **1e** did not show any G2 block. Stacey and co-workers have provided evidence that the level of cyclin D1 is high in the G1 phase and low in the S phase, to allow the synthesis of DNA, and then again high in the G2 phase, to promote continuing cell cycle progression. Since cyclin D1 should return high in the G2 phase, we expected that the blockade of the cells in the G2 phase is associated with a low level of cyclin D1. By immunoblotting, we therefore determined the level of cyclin D1 48 h after treatment with **3a** and **3c**, when the cells were blocked in G2. We found indeed that cyclin D1 was reduced to <10% of the control (Figure 8B). Since p21[RAS] is also inhibited to <30% of the control 48 h after treatment with **3a** and **3c** (Figure 5B), our data also suggest that there is a correlation between the level of cyclin D1 and *HRAS* activity. These results are in keeping with the observed blockade of the cell cycle.

Compound 3a Inhibits Tumor Growth and Increases the Survival of Nude Mice Carrying a T24 Tumor Xenograft. The activity of compound **3a**, which shows in vitro the strongest capacity to suppress *HRAS* and cell growth, was assessed also in vivo in nude mice bearing a T24 tumor xenograft. The mice bearing a subcutaneous T24 tumor of 180−250 mm³ were randomly divided into two groups of eight

mice each. One group was intratumorally injected with a 50 μL solution containing a low dose of compound **3a** (1.7 mg/kg). This treatment was repeated four times (at days 1, 8, 15, and 22), and the tumor size was measured every 2−3 days with a caliper. The results are reported in Figure 8C (left). It can be seen that compound **3a** significantly reduced the growth of the xenograft compared with the nontreated group. In particular, after the second treatment at day 8, the size of the tumor in the two groups was statistically different with $P < 0.05$. But after the third treatment the difference in tumor size became more pronounced with $P < 0.001$. Figure 8C (right) reports the Kaplan−Meier survival curves for the two groups of mice. The median survival time for the untreated group was 32 days, while it was 54 days for the group treated with **3a**, i.e., increased by ~70% compared with the control group ($P < 0.0001$).

■ CONCLUSIONS

In this work we have documented that chloroacetamidine-containing anthrathiophenediones represent a class of compounds showing a challenging anti *HRAS* activity. The lead compounds **3a** and **3c** bind tightly to the G-quadruplexes controlling the expression of *HRAS* and promote the downregulation of the oncogene in bladder cancer cells. The designed chloroacetamidine-containing compounds are taken up by bladder cancer cells much more efficiently than the corresponding analogues with guanidine-containing side chains. This is probably due to the fact that the former compounds are more lipophilic and have positive charges in the side chains that are less stabilized by resonance. Contrary to the guanine-containing analogues, compounds **3a** and **3c** induce a strong apoptotic response in T24 cancer cells, leading to the arrest of cell growth. The compounds down-regulate cyclin D1 and block the cells in the G2 phase. Finally, compound **3a** injected intratumorally in nude mice bearing a T24 xenograft inhibited tumor growth and increased the median survival time, from 32 to 54 days. Together, our data suggest that the designed chloroacetamidine-containing anthrathiophenediones may have potential in the treatment of human bladder cancer.

■ MATERIALS AND METHODS

General Methods. NMR spectra were registered on a Varian VXR-400 instrument operated at 400 MHz (^{1}H NMR) and 100 MHz (^{13}C NMR). Chemical shifts were measured in CD$_3$OD or DMSO-d_6 using tetramethylsilane as internal standard. Analytical TLC was performed on silica gel F$_{254}$ plates (Merck) and column chromatography on silica gel Merck 60 silanized. Melting points were determined on a Buchi SMP-20 apparatus and are uncorrected. High-resolution mass spectra were recorded with electrospray ionization on a Bruker Daltonics micrOTOF-QII instrument. UV spectra were recorded on a Hitachi-U2000 spectrophotometer. HPLC was performed using Shimadzu CLASS-VP V6.12SP1 system (Kromasil-100-5-mkm C-18 column, 4.6 mm × 250 mm); eluent A, H$_3$PO$_4$ (0.01 M); eluent B, MeCN. All solutions were evaporated at reduced pressure on a Buchi-R200 rotary evaporator at a temperature below 45 °C. All products were vacuum-dried at room temperature. All solvents, chemicals, and reagents were obtained commercially and used without purifications. Anthra[2,3-*b*]thiophen-5,10-diones **2a−e** were prepared as described early.[9,12] The purity of all anthra[2,3-*b*]thiophen-5,10-diones **3a−e** was determined as >95% by

HPLC analysis, and for compound **3a** it was additionally confirmed by elemental analysis.

4,11-Bis[2-(chloroacetamidine)ethylamino]anthra-[2,3-*b*]thiophene-5,10-dione Dihydrochloride (3a). To a stirring solution of free base of 4,11-bis[(2-aminoethyl)amino]-anthra[2,3-*b*]thiophene-5,10-dione[12] (**2a**, 110 mg, 0.3 mmol) in DMSO (10.0 mL), methanol (10.0 mL), ethyl 2-chloroacetimidate hydrochloride (0.2 g, 1.3 mmol), and triethylamine (0.16 mL, 1.1 mmol) were subsequently added. The mixture was stirred for 3 h at 45 °C, then cooled and quenched with acetone. The dark blue precipitate was collected by filtration and purified by reverse phase chromatography (H$_2$O−MeCN−HCO$_2$H, 50:10:1 v/v). The residue obtained after purification and evaporation was dissolved in warm MeOH. Then a solution of 1 N HCl in MeOH (0.5 mL) was added and the product was reprecipitated with acetone. The solid was collected, washed with acetone and, after drying, yielded dihydrochloride **3a**. Yield 77 mg (44%); mp 245−247 °C (dec); HPLC (LW = 564 nm, gradient B 15% → 40% (30 min)) t_R = 11.87 min; purity 97.1%. ^{1}H NMR (400 MHz, CD$_3$OD) δ 8.18 (2H, m, 6-H, 9-H), 7.98 (1H, d, J = 7.8 Hz, 3-H), 7.89 (1H, d, J = 7.8 Hz, 2-H), 7.67 (2H, m, 7-H, 8-H), 4.43 (4H, s, CH$_2$Cl), 4.15 (2H, m, HNCH_2), 4.00 (2H, m, HNCH_2), 3.73 (2H, m, CH_2NH); ^{1}H NMR (400 MHz, DMSO-d_6) δ 11.92 (br s, 2H, 2NHCH$_2$), 10.71 (m, 2H, 2NH), 9.99 (d, 2H, J = 6.9 Hz, =NH$_2$), 9.66 (d, 2H, J = 8.6 Hz, =NH$_2$), 8.17 (m, 3H, 2-H, 7-H, 8-H), 7.95 (d, 1H, J = 5.5 Hz, 3-H), 7.73 (m, 2H, 6-H, 9-H), 4.54 (s, 2H, CH$_2$Cl), 4.53 (s, 2H, CH$_2$Cl), 4.09 (m, 2H, HNCH_2), 3.95 (m, 2H, HNCH_2), 3.72 (m, 4H, 2CH_2NH). ^{13}C NMR (100 MHz, DMSO-d_6) δ 180.7 (2C=O), 162.95 (C), 162.88 (C), 146.01 (C), 145.14 (C), 135.52 (C), 135.23 (C), 133.98 (C), 133.85 (C), 108.15 (C), 106.76 (C), 132.35 (2CH), 131.42 (CH), 126.01 (CH), 125.78 (2CH), 45.00 (CH$_2$), 43.23 (CH$_2$), 42.98 (CH$_2$), 42.97 (CH$_2$), 38.91 (2CH$_2$). HRMS (ESI) calculated for C$_{24}$H$_{25}$Cl$_2$N$_6$O$_2$S [M + H]$^+$ 531.1131, found 531.1040. Anal. Calcd for C$_{24}$H$_{24}$Cl$_2$N$_6$O$_2$S·2HCl·2H$_2$O: C, 45.01; H, 4.72; N, 13.12; S, 5.01. Found, %: C, 45.22; H, 4.45; N, 13.02; S, 5.13.

4-[2-(Chloroacetamidine)ethylamino]-11-[3-(chloroacetamidine)propylamino]anthra[2,3-*b*]-thiophene-5,10-dione Dihydrochloride (3b). This compound was prepared from 4-[(2-aminoethyl)amino]-11-[(3-aminopropyl)amino]anthra[2,3-*b*]thiophene-5,10-dione (**2b**)[9] as described for **3a**. Dark blue powder, yield 41%, mp 224−226 °C (dec). HPLC (LW = 564 nm, gradient B 15% → 40% (30 min)) t_R = 14.28 min, purity 96.0%. ^{1}H NMR (400 MHz, CD$_3$OD) δ 8.13 (2H, d, 6-H, 9-H), 7.96 (1H, d, J = 5.8 Hz, 3-H), 7.85 (1H, d, J = 5.8 Hz, 2-H), 7.64 (2H, m, 7-H, 8-H), 4.45 (2H, s, CH$_2$Cl), 4.42 (2H, s, CH$_2$Cl), 3.98 (4H, m, 2HNCH_2), 3.72 (2H, t, J = 5.8 Hz, CH_2NH), 3.58 (2H, t, J = 6.8 Hz, CH_2NH), 2.16 (2H, m, CH$_2$). HRMS (ESI) calculated for C$_{25}$H$_{27}$Cl$_2$N$_6$O$_2$S [M + H]$^+$ 545.1288, found 545.1279.

11-[2-(Chloroacetamidine)ethylamino]-4-[3-(chloroacetamidine)propylamino]anthra[2,3-*b*]-thiophene-5,10-dione Dihydrochloride (3c). This compound was prepared from 11-[(2-aminoethyl)amino]-4-[(3-aminopropyl)amino]anthra[2,3-*b*]thiophene-5,10-dione (**2c**)[9] as described for **3a**. Dark blue powder, yield 43%, mp 211−212 °C (dec). HPLC (LW = 564 nm, gradient B 15% → 40% (30 min)) t_R = 14.38 min, purity 96.8%. ^{1}H NMR (400 MHz, CD$_3$OD) δ 8.19 (2H, m, 6-H, 9-H), 8.07 (1H, d, J = 5.8 Hz, 3-H), 8.01 (1H, d, J = 5.8 Hz, 2-H), 7.71 (2H, m, 7-H, 8-H), 4.45 (2H, s, CH$_2$Cl), 4.43 (2H, s, CH$_2$Cl), 4.22 (2H, m, HNCH_2),

3.82 (2H, m, HNCH$_2$), 3.77 (2H, t, J = 5.9 Hz, CH$_2$NH), 3.56 (2H, t, J = 6.9 Hz, CH$_2$NH), 2.28 (2H, m, CH$_2$). HRMS (ESI) calculated for C$_{25}$H$_{27}$Cl$_2$N$_6$O$_2$S [M + H]$^+$ 545.1288, found 545.1273.

4,11-Bis[3-(chloroacetamidine)propylamino]anthra-[2,3-*b*]thiophene-5,10-dione Dihydrochloride (3d). This compound was prepared from 4,11-bis[(3-aminopropyl)-amino]anthra[2,3-*b*]thiophene-5,10-dione (**2d**)[9] as described for **3a**. Dark blue powder, yield 43%, mp 207−208 °C (dec). HPLC (LW = 564 nm, gradient B 15% → 40% (30 min)) t_R = 15.06 min, purity 95.9%. ^{1}H NMR (400 MHz, CD$_3$OD) δ 8.15 (2H, m, 6-H, 9-H), 8.03 (2H, m, 2-H, 3-H), 7.70 (2H, m, 7-H, 8-H), 4.45 (2H, s, CH$_2$Cl), 4.43 (2H, s, CH$_2$Cl), 3.80 (2H, m, HNCH$_2$), 3.65 (6H, m, HNCH$_2$, 2CH$_2$NH), 2.21 (4H, m, 2CH$_2$). HRMS (ESI) calculated for C$_{26}$H$_{29}$Cl$_2$N$_6$O$_2$S [M + H]$^+$ 559.1444, found 559.1432.

4,11-Bis[4-(chloroacetamidine)butylamino]anthra-[2,3-*b*]thiophene-5,10-dione Dihydrochloride (3e). This compound was prepared from 4,11-bis[(4-aminobutyl)amino]-anthra[2,3-*b*]thiophene-5,10-dione (**2e**)[9] as described for **3a**. Dark blue powder, yield 33%, mp 196−198 °C (dec). HPLC (LW = 564 nm, gradient B 15% → 40% (30 min)) t_R = 16.88 min, purity 97.4%. ^{1}H NMR (400 MHz, CD$_3$OD) δ 8.21 (2H, m, 6-H, 9-H), 8.03 (1H, d, J = 6.8 Hz, 3-H), 7.95 (1H, d, J = 6.8 Hz, 2-H), 7.70 (2H, m, 7-H, 8-H), 4.42 (4H, s, CH$_2$Cl), 3.73 (4H, m, 2HNCH$_2$), 3.45 (4H, m, CH$_2$NH), 1.91 (8H, m, 2(CH$_2$)$_2$). HRMS (ESI) calculated for C$_{28}$H$_{33}$Cl$_2$N$_6$O$_2$S [M + H]$^+$ 587.1757, found 587.1763.

Oligonucleotides. HPLC-purified oligonucleotides used in this study have been obtained from Microsynth AG (Switzerland). Melting experiments have been performed with a real-time PCR apparatus using dual-labeled oligonucleotides FAM-TCGGGTTGCGGGCGCAGGGCACGGGCG-TAMRA (*hras*-1) and FAM-CGGGGCGGGGCGGGGGCGGG-GGCG-TAMRA (*hras*-2).

Cell Culture, Metabolic Activity, and Proliferation Assays. T24 urinary bladder cancer and 293 human kidney embryonic cells were maintained in exponential growth in Dulbecco's modified Eagle medium (DMEM) containing 100 U/mL penicillin, 100 mg/mL streptomycin, 20 mM L-glutamine, and 10% fetal bovine serum (Euroclone, Milan, Italy). For metabolic assays, the cells were seeded (10 000 or 30 000 cells/well) the day before CATD treatment in a 96-well plate. Metabolic activity was measured by resazurin assays following standard procedures at the time indicated.

For proliferative assay, 500 cells were plated in a 60 mm plate and treated with 1 μM CATDs. After 7 days of treatment cells were fixed and stained for 10 min in 2.5% methylene blue in 50% ethanol. Colonies composed of more than 50 cells were counted.

FACS Analysis. T24 bladder cancer and 293 noncancer cells have been plated in a 24-well plate at a density of 5×10^4 or 15×10^4 cells/well, respectively. After 1 day, the cells were treated with the designed CATDs: time and concentration are as indicated in figure captions.

For uptake studies, the cells have been treated for 4 h with CATDs (1 and 5 μM). After incubation, the cells were trypsinized and pelleted. The pellets were resuspended in 200 μL of PBS and immediately analyzed by FACSCalibur flow cytometer (Becton-Dickinson, San Jose, CA, USA) equipped with a single 488 nm argon laser. A minimum of 10 000 cells for each sample were acquired. The cell population was analyzed by FSC light and SSC light. The signal was detected by FL3

(680 nm) channel in log scale. Uptake in the presence of dynasore was performed by treating the cells for 30 min with 80 μM dynasore before the CATDs were added.

For the cell cycle analyses the cells have been incubated with 5 μM **3a**, **3c**, **1a**, and **1e** for 48 or 72 h. After incubation the dead floating cells were collected and the adherent cells were trypsinized. All cells were combined, fixed for 1 h at 4 °C in 70% ethanol, 30% PBS. After fixing, the cells were washed with PBS and stained with 0.05 mg/mL propidium iodide in the presence of 0.1 mg/mL RNase A in PBS (30 min at room temperature). The cell samples were analyzed by FACS (FL2 channel 585 nm). The cell cycle data have been obtained with FLOWJO flow cytometry analysis software (FLOWJO LLC, Ashland OR USA).

Annexin V−propidium iodide assay was performed by using annexin V apoptosis detection kit (Santa Cruz Biotechnology Inc., Dallas, TX) and following the manufacturer's instructions. Briefly, the cells were harvested by trypsinization (adherent cells) and by centrifugation (floating cells) and all cells were resuspended in a buffer containing propidium iodide and FITC-conjugated antibody specific for annexin V. After 15 min of incubation in the dark, the cells were analyzed with the cytofluorimeter either in FL1 (530 nm) for annexin V or in FL2 (585 nm) for propidium iodide.

Confocal Microscopy. T24 bladder cancer cells were plated (3×10^5) on a coverslip placed in a Petri dish (diameter 35 mm) and after 24 h treated with 5 μM CATD for 4 h. The cells were washed twice with PBS, fixed with 3% paraformalde-hyde (PFA) in PBS for 20 min. After washing with 0.1 M glycine, containing 0.02% sodium azide in PBS to remove PFA and Triton X-100 (0.1% in PBS), the cells were incubated for 1 h with DRP1 antibody (Santa Cruz Biotechnology) diluted 1:250 in PBS and then 30 min with secondary mouse IgG FITC (Biolegend) diluted 1:250 in PBS. For untreated cells, the nuclei were stained for 30 min with propidium iodide (3 ng/μL, 0.4 μg/mL RNase A in PBS). The cells were analyzed using a Leica TCS SP1 confocal imaging system.

FRET Experiments. FRET experiments with oligonucleo-tides *hras*-1 and *hras*-2, tagged at the 5′ and 3′ ends with FAM and TAMRA, were carried out on a microplate spectrofluor-ometer system (PerkinElmer 2300 Enspire, USA). Each sample contained 50 μL of dual-labeled oligonucleotide (200 nM) in 50 mM Tris buffer, pH 7.4, 100 mM KCl for *hras*-1, and 10 mM for *hras*-2. The samples were incubated as specified in the text. Emission spectra were obtained setting the excitation wavelength at 480 nm and recording the emission from 500 to 650 nm. FRET-melting experiments were performed on a real-time PCR apparatus (CFX96, BioRad, Hercules, CA). FRET-melting experiments were obtained as follows: equilibration at 20 °C for 5 min, stepwise increase of temperature up to 95 °C (1 °C/min), 76 cycles.

RNA Extraction and Real-Time PCR. T24 bladder cells were plated in 96-well plate (10^4 cells/well). After 24 h, RNA was extracted by using iScript RT-qPCR sample preparation reagent (BioRad, USA).

For cDNA synthesis, 1.25 μL of RNA was heated at 70 °C and placed in ice. To the solution was added 7.5 μL of a mix containing (final concentrations) 1× buffer; 0.01 M DTT (Invitrogen); 1.6 μM primer dT [MWG Biotech, Ebersberg, Germany; d(T)16]; 1.6 μM random primers; 0.4 mM dNTPs solution containing equimolar amounts of dATP, dCTP, dGTP, and dTTP (Euroclone, Pavia, Italy); 0.8 U/μL RNase OUT; 8 U/μL of M-MLV reverse transcriptase (Life

Technologies, Monza, Italy). The reactions were incubated for 1 h at 37 °C and stopped by heating at 95 °C for 5 min. As a negative control, the reverse transcription reaction was performed with a sample containing DEPC water.

Real-time PCR multiplex reactions were performed with 1× Kapa Probe fast qPCR kit (KAPA Biosystems, Wilmington, MA, USA) for HRAS and housekeeping gene β2-microglobulin, 2.2 μL of cDNA, and primers/probes at the following concentrations: for HRAS accession code NM 001130442, probe FAM-CAATGACCACCTGCTTCCG-BHQ1 (from 309 to 327, 260 nM), primer sense 5′-GCTGATCCAGAAC-CATTT (from 254 to 271, 340 nM), primer antisense 5′-GTATCCAGGATGTCCAAC (from 344 to 361, 260 nM); for β2-microglobulin accession code NM 004048, probe ROX-TATGCCTGCCGTGTGAACC-BHQ2 (from 352 to 370, 60 nM), primer sense 5′-CCCCACTGAAAAAGATGA (from 333 to 350, 100 nM), primer antisense 5′-CCATGATGCTGCTT-ACAT (from 415 to 432, 100 nM). The PCR cycle was 3 min at 95 °C, 50 cycles 10 s at 95 °C, 60 s at 58 °C. PCR reactions were carried out with a CFX-96 real-time PCR apparatus controlled by an Optical System software (version 3.1) (Bio-Rad Laboratories, CA, USA). All expressions were normalized with housekeeping gene.

Western Blots. Total protein lysates (20 μg) were electrophoresed on 12% SDS−PAGE and transferred to a nitrocellulose membrane at 70 V for 2 h. The filter was blocked for 1 h with 5% solution nonfat dry milk in PBS, 0.05% Tween (Sigma-Aldrich, Milan, Italy) at room temperature. The primary antibodies used are from Cell Signaling (CS) unless differently indicated: anti-actin (IgM mouse 1:10 000 ab-1 Calbiochem), anti-Hras (IgG rabbit 1:500 ab32417 Abcam), anti-phospho-p44-42 MAPK (Erk1/2) (IgG rabbit 1:1000 Thr202/Tyr204 CS), anti-p44/42 MAPK (Erk1/2) (IgG rabbit 1:1000 CS), anti-PARP (IgG rabbit 1:1000 CS) anti-phospho-Akt (IgG rabbit 1:1000 CS), anti-cyclin D1 (IgG mouse 1:2000 CS), and anti-Akt (IgG rabbit 1:1000 CS). Membranes with the samples were overnight incubated at 4 °C with primary antibodies. The filters were washed with a 0.05% Tween in PBS and subsequently incubated for 1 h with a secondary antibody conjugated with horseradish peroxidase: anti-rabbit IgG or anti-mouse IgM or anti-mouse IgG, diluted 1:5000 (Calbiochem). For the detection of the proteins we used Super SignalWest PICO and FEMTO (Thermo Fisher Scientific Pierce). Exposure length depends on the antibodies used.

Apo-ONE Assay. Caspase activity assay was performed with Apo-ONE homogeneous caspase-3/7 assay (Promega), according to the manufacturer's protocol.

Human Tumor Xenograft Model in Nude Mice. Nude mice of ∼20 g were implanted subcutaneously with human T24 cells (15 × 10⁶ cells) in 100 μL of physiological solution using a 23-gauge needle. Each mouse received one injection in the right flank for the development of a tumor xenograft in 6−7 weeks. Treatment with compound **3a** started when the tumor had a size between 180 and 1050 mm³. The mice were randomized into two groups of eight animals, and compound **3a** was injected intratumorally (1.7 mg/kg). Each mouse of the treated group received four doses of compound **3a** at days 1, 8, 15, and 22. The tumor growth was measured with a caliper. Tumor volume was calculated according to $V = [(\text{small diameter})^2 \times (\text{large diameter})]\pi/6$ every 2−3 days up to 44 days since the first treatment. The tumor volume (cm³) was transformed into mass (mg), assuming a density of 1. All procedures involving the animals have been approved by the Italian Ministry of Health (D.M. n. 67/2013-B dd. 19/03/2013) and by the Ethical Committee of the University of Trieste (Prot. 569/2013).

Statistical Analyses. The primary growth tumor analyses were performed by using GraphPad Prism. Tabled values are group mean values $\pm$ SE (standard error). Data were subjected to the appropriate factorial ANOVA assessing significance against an α-level $p < 0.05$. When the individual effect of the treatments and the interaction between the independent variables in a 2 × 2 ANOVA was significant, the data were subjected to post hoc Tukey test for significance of the differences in the mean values. All analyses were performed using standard procedures implemented in the Systat package (SYSTAT Inc., Evanston, IL). The survival analysis was performed using the Kaplan−Meier curve (SPSS 11.0 for Windows 2000 software), and the p values were calculated by long-rank test.

■ ASSOCIATED CONTENT

ⓢ Supporting Information

Absorbance and fluorescence spectra of **3a** and **3c**; fluorescence titrations of quadruplex hras-2 tagged with FAM and TAMRA; structure of guanidine-containing anthrathiophenediones **1a** and **1e**; annexin-propidium iodide data; cell cycle of T24 cells treated with **3a**, **3c**, **1a**, and **1e**; csv file containing molecular formula strings. The Supporting Information is available free of charge on the online version of the article.

■ AUTHOR INFORMATION

Corresponding Author
*E-mail: luigi.xodo@uniud.it. Phone: (+39)0432494395. Fax: (+39)0432494301.

Author Contributions
The manuscript was written through contributions of all authors. All authors have given approval to the final version of the manuscript.

Notes
The authors declare no competing financial interest.

■ ACKNOWLEDGMENTS

■ ABBREVIATIONS USED

CATD, 4,11-bis[ω-(chloroacetamidine)alkylamino]anthrathio-phenedione; FRET, fluorescence resonance energy transfer; DRP-1, dynamin related protein 1

■ REFERENCES

(1) Fizazi, K.; De Bono, J. S.; Flechon, A.; Heidenreich, A.; Voog, E.; Davis, N. B.; Qi, M.; Bandekar, R.; Vermeulen, J. T.; Cornfeld, M.; Hudes, G. R. Randomised phase II study of siltuximab (CNTO 328), an anti-IL-6 monoclonal antibody, in combination with mitoxantrone/prednisone versus mitoxantrone/ prednisone alone in metastatic castration-resistant prostate cancer. *Eur. J. Cancer* **2012**, 48, 85−89.
(2) Faulds, D.; Balfour, J. A.; Chrisp, P.; Langtry, H. D. Mitoxantrone. A review of its pharmacodynamic and pharmacokinetic properties, and therapeutic potential in the chemotherapy of cancer. *Drugs* **1991**, 41, 400−449.

(3) Gewirtz, D. A. A critical evaluation of the mechanisms of action proposed for the antitumor effects of the anthracycline antibiotics adriamycin and daunorubicin. *Biochem. Pharmacol.* **1999**, *57*, 727−741.

(4) (a) Xie, G.; Zhu, X.; Li, Q.; Gu, M.; He, Z.; Wu, J.; Li, J.; Lin, Y.; Li, M.; She, Z.; Yana, J. SZ-685C, a marine anthraquinone, is a potent inducer of apoptosis with anticancer activity by suppression of the Akt/FOXO pathway. *Br. J. Pharmacol.* **2010**, *159*, 689−697. (b) Ma, J.; Lu, H.; Wang, S.; Chen, B.; Liu, Z.; Ke, X.; Liu, T.; Fu, J. The anthraquinone derivative Emodin inhibits angiogenesis and metastasis through downregulating Runx2 activity in breast cancer. *Int. J. Oncol.* **2015**, *46*, 1619−1628. (c) Tang, S. H.; Huang, H. S.; Wu, H. U.; Tsai, Y. T.; Chuang, M. J.; Yu, C. P.; Huang, S. M.; Sun, G. H.; Chang, S. Y.; Hsiao, P. W.; Yu, D. S.; Cha, T. L. Pharmacologic down-regulation of EZH2 suppresses bladder cancer in vitro and in vivo. *Oncotarget* **2014**, *15*, 10342−1055.

(5) Sun, D.; Thompson, B.; Cathers, B. E.; Salazar, M.; Kerwin, S. M.; Trent, J. O.; Jenkins, T. C.; Neidle, S.; Hurley, L. H. Inhibition of human telomerase by a G-quadruplex-interactive compound. *J. Med. Chem.* **1997**, *40*, 2113−2116.

(6) Perry, P. J.; Reszka, A. P.; Wood, A. A.; Read, M. A.; Gowan, S. M.; Dosanjh, H. S.; Trent, J. O.; Jenkins, T. C.; Kelland, L. R.; Neidle, S. Human telomerase inhibition by regioisomeric disubstituted amidoanthracene-9,10-diones. *J. Med. Chem.* **1998**, *41*, 4873−4884.

(7) (a) Teulade-Fichou, M.-P.; Housou, C.; Guittat, L.; Hoarau, M.; Arimondo, P. B.; Vigneron, J.-P.; Lehn, J.-M.; Riou, J.-F.; Garestier, T.; Héíeɴe, C. Telomerase inhibitors based on quadruplex ligands selected by a fluorescence assay. *Proc. Natl. Acad. Sci. U.S.A.* **2001**, *98*, 3062−3067. (b) Alcaro, S.; Artese, A.; Iley, J. N.; Missailidis, S.; Ortuso, F.; Parrotta, L.; Pasceri, R.; Paduano, F.; Sissi, C.; Trapasso, F.; Vigorita, M. G. Rational design, synthesis, biophysical and antiproliferative evaluation of fluorenone derivatives with DNA G-quadruplex binding properties. *ChemMedChem* **2010**, *5*, 575−583. (c) Perry, P. J.; Read, M. A.; Davies, R. T.; Gowan, S. M.; Reszka, A. P.; Wood, A. A.; Kelland, L. R.; Neidle, S. 2,7-Disubstituted amidofluorenone derivatives as inhibitors of human telomerase. *J. Med. Chem.* **1999**, *42*, 2679−2684.

(8) Neidle, S.; Harrison, R. J.; Reszka, A. P.; Read, M. A. Structure-activity relationships among guanine-quadruplex telomerase inhibitors. *Pharmacol. Ther.* **2000**, *85*, 133−139.

(9) Cogoi, S.; Shchekotikhin, A. E.; Membrino, A.; Sinkevich, Y. B.; Xodo, L. E. Guanidine anthrathiophenediones as G-quadruplex binders: uptake, intracellular localization, and anti-Harvey-ras gene activity in bladder cancer cells. *J. Med. Chem.* **2013**, *56*, 2764−2778.

(10) Zagotto, G.; Sissi, C.; Lucatello, L.; Pivetta, C.; Codamuro, S. A.; Fox, K. R.; Neidle, S.; Palumbo, M. Aminoacyl-anthraquinone conjugates as telomerase inhibitors: synthesis, biophysical and biological evaluation. *J. Med. Chem.* **2008**, *51*, 5566−5574.

(11) Ilyinsky, N. S.; Shchyolkina, A. K.; Borisova, O. F.; Mamaeva, O. K.; Zvereva, M. I.; Azhibek, D. M.; Livshits, M. A.; Mitkevich, V. A.; Balzarini, J.; Sinkevich, Y. B.; Luzikov, Y. N.; Dezhenkova, L. G.; Kolotova, E. S.; Shtil, A. A.; Shchekotikhin, A. E.; Kaluzhny, D. N. Novel multi-targeting anthra[2,3-b]thiophene-5,10-diones with guanidine-containing side chains: interaction with telomeric G-quadruplex, inhibition of telomerase and topoisomerase I and cytotoxic properties. *Eur. J. Med. Chem.* **2014**, *85*, 605−614.

(12) Shchekotikhin, A. E.; Glazunova, V. A.; Dezhenkova, L. G.; Luzikov, Y. N.; Sinkevich, Y. B.; Kovalenko, L. V.; Buyanov, V. N.; Balzarini, J.; Huang, F. C.; Lin, J. J.; Huang, H. S.; Shtil, A. A.; Preobrazhenskaya, M. N. Synthesis and cytotoxic properties of 4,11-bis[(aminoethyl)amino]anthra[2,3-b]thiophene-5,10-diones, novel analogues of antitumor anthracene-9,10-diones. *Bioorg. Med. Chem.* **2009**, *17*, 1861−1869.

(13) Blum, R.; Kloog, Y. Metabolism addiction in pancreatic cancer. *Cell Death Dis.* **2014**, *5*, e1065.

(14) Locasale, J. W.; Cantley, L. C.; Vander Heiden, M. G. Cancer's insatiable appetite. *Nat. Biotechnol.* **2009**, *27*, 916−917.

(15) Cogoi, S.; Shchekotikhin, A. E.; Xodo, L. E. HRAS is silenced by two neighboring G-quadruplexes and activated by MAZ, a zinc-finger transcription factor with DNA unfolding property. *Nucleic Acids Res.* **2014**, *42*, 8379−8388.

(16) Membrino, A.; Cogoi, S.; Pedersen, E. B.; Xodo, L. E. G4-DNA formation in the HRAS promoter and rational design of decoy oligonucleotides for cancer therapy. *PLoS One* **2011**, *6*, e24421.

(17) Macia, E.; Ehrlich, M.; Massol, R.; Boucrot, E.; Brunner, C.; Kirchhausen, T. Dynasore a cell permeable inhibitor of dynamin. *Dev. Cell* **2006**, *10*, 839−850.

(18) Tsai, C. C.; Lin, C. L.; Wang, T. L.; Chou, A. C.; Chou, M. Y.; Lee, C. H.; Peng, I. W.; Liao, J. H.; Chen, Y. T.; Pan, C. Y. Dynasore inhibits rapid endocytosis in bovine chromaffin cells. *Am. J. Physiol.* **2009**, *297*, 397−406.

(19) Iacoppetta, B. J.; Morgan, E. H. The kinetics of transferrin endocytosis and iron uptake from transferrin in rabbit reticulocytes. *J. Biol. Chem.* **1983**, *258*, 9108−9115.

(20) Thoms, S.; Eldermann, R. Dynamin-related proteins and Pex11 proteins in peroxisome division and proliferation. *FEBS J.* **2005**, *272*, 5169−5181.

(21) Frank, S.; Gaume, B.; Bergmann-Leitner, E. S.; Leitner, W. W.; Everett, G. R.; Catez, F.; Smith, C. L.; Youle, R. J. The role of dynamin-related protein 1, a mediator of mitochondrial fission in apoptosis. *Dev. Cell* **2001**, *1*, 515−525.

(22) Lowy, D. R.; Willumsen, B. M. Function and regulation of ras. *Annu. Rev. Biochem.* **1993**, *62*, 851−891.

(23) Tsai, F. M.; Shyu, R. Y.; Jiang, S. Y. RIG1 inhibits the Ras/mitogen-activated protein kinase pathway by suppressing the activation of Ras. *Cell. Signalling* **2006**, *18*, 349−358.

(24) D'Amours, D.; Sallmann, F. R.; Dixit, V. M.; Poirier, G. G. Gain-of-function of poly(ADP-ribose) polymerase-1 upon cleavage by apoptotic proteases: implications for apoptosis. *J. Cell Sci.* **2001**, *114*, 3771−3778.

(25) Savatier, J.; Rharass, T.; Canal, C.; Gbankoto, A.; Vigo, J.; Salmon, J. M.; Ribou, A. C. Adriamycin dose and time effects on cell cycle, cell death and reactive oxygen species generation in leukaemia cell. *Leuk. Res.* **2012**, *36*, 791−798.

(26) Lo, Y. L.; Wang, W. Formononetin potentiates epirubicin-induced apoptosis via ROS production in HeLa cells in vitro. *Chem.-Biol. Interact.* **2013**, *205*, 188−197.

(27) Marczak, A.; Bukowska, B. ROS production and their influence on the cellular antioxidative system in human erythrocytes incubated with daunorubicin and glutaraldehyde. *Environ. Toxicol. Pharmacol.* **2013**, *36*, 171−181.

(28) Montoya, S. C.; Comini, L. R.; Sarmiento, M.; Becerra, C.; Albesa, I.; Argüellom, G. A.; Cabrera, J. L. Natural anthraquinones probed as type I and type II photosensitizers: singlet oxygen and superoxide anion production. *J. Photochem. Photobiol., B* **2005**, *78*, 77−83.

(29) Stacey, D. W. Cyclin D1 serves as a cell cycle regulatory switch in actively proliferating cells. *Curr. Opin. Cell Biol.* **2003**, *15*, 158−163.

(30) Sherr, C. J. D-Type cyclins. *Trends Biochem. Sci.* **1995**, *20*, 187−190.

(31) Hitomi, M.; Stacey, D. W. Cyclin D1 production in cycling cells depends on Ras in a cell-cycle-specific manner. *Curr. Biol.* **1999**, *9*, 1075−1084.

(32) Hitomi, M.; Stacey, D. W. Cellular ras and cyclin D1 are required during different cell cycle periods in cycling NIH 3T3 cells. *Mol. Cell. Biol.* **1999**, *19*, 4623−4632.

(33) Mulcahy, L. S.; Smith, M. R.; Stacey, D. W. Requirement for ras protooncogene function during serum stimulated growth oh NIH 3T3 cells. *Nature* **1985**, *313*, 241−243.

(34) Moodie, S. A.; Wolfman, A. The 3Rs of life: raf, ras and growth regulation. *Trends Genet.* **1994**, *10*, 44−48.